Catalysis Science & Technology

ROYAL SOCIETY OF CHEMISTRY

PAPER

View Article Online
View Journal

Cite this: DOI: 10.1039/d6cy00261g

On the reactions of (hetero)aryl and vinyl triflates with [Ni(COD)(dppf)]

Nicholas C. C. McVeigh, †[a] Megan E. Greaves,†‡[a] Rachel H. Munday,[b] Thomas O. Ronson, [b] Scott Rice,[b] Stephen Sproules [c] and David J. Nelson *[a]

Received 2nd March 2026,
Accepted 4th May 2026

DOI: 10.1039/d6cy00261g

rsc.li/catalysis

We report the experimental and computational investigations of the reactions of aryl, heteroaryl, and vinyl triflates with a model nickel(0) complex. While the reactions of most (hetero)aryl and vinyl triflates behave straightforwardly, the reactions of 2-pyridinyl triflates are rather different; under reaction conditions where the organotriflates are used in vast excess there is not a simple pseudo-first order behaviour. These reactions are further explored using DFT calculations, which show that both three- and five-centred oxidative addition transition states are viable, but that the experimentally-observed order of reactivity is not readily reproduced by considering a simple oxidative addition pathway.

Introduction

Organotriflates are substrates for many nickel-catalysed reactions.[1–6] They are readily synthesised from the corresponding alcohols or enolisable ketones, and are often substantially more reactive than alternative alcohol derivatives.[7]

The reactions of a range of nickel(0) complexes with organohalides have been studied in some depth,[8] but less is known about the mechanisms of the reactions of aryl and vinyl triflates with nickel(0). This is in contrast with palladium, for which there are many such studies; a discussion of all such studies would be beyond the scope of this manuscript, but we note in particular some seminal work by Maes and Jutand,[9] and recent work by Neufeldt[10] and by Leitch[11,12] (*vide infra*).

We have previously studied the reactions of a range of aryl (pseudo)halides with [Ni(COD)(dppf)] (**1**),[13] which is a convenient, thermally stable, catalytically active model nickel(0) species (COD = 1,5-cyclooctadiene; dppf = 1,1′-bis(diphenylphosphino)ferrocene).[14] We have studied the reactions of **1** with (hetero)aryl[13,15,16] and alkyl[17,18] halides, and ranked a series of aryl substrates of the form *p*-(F_3C)C_6H_4X in order of their reactivity with **1**.[13] Somewhat surprisingly, **1** undergoes reaction with *p*-(F_3C)C_6H_4OTf (**2a**) more slowly than with *p*-(F_3C)C_6H_4OTs (**3a**). Recently, we noted that the reaction of 2-pyridyl triflate (**2b**) with **1** forms [Ni(κ²-*C*,*N*-2-pyridyl)(dppf)][OTf] (**4**) in which the triflate moiety is present as an outer-sphere counterion to a pseudo-square planar cationic nickel(II) complex.[16]

Neufeldt and colleagues have studied the reactions of aryl sulfonates with nickel(0) in some depth.[19,20] They noted that selectivity for aryl tosylate *versus* aryl chloride oxidative addition could be modulated *via* judicious ligand selection; nickel complexes with most widely-used phosphine ligands preferentially activate aryl chlorides, while complexes of trimethylphosphine show the opposite selectivity, by lowering the energy of the five-centre oxidative addition transition state for aryl tosylates.[19]

The triflate anion is often only weakly coordinating to transition metals, which is exploited in regiocontrol during Heck reactions. There is evidence that the triflate anion is also weakly bound in arylnickel(II) triflate complexes on the basis of broad ^{31}P NMR spectra that sharpen on the addition of bromide.[13]

Organotriflates may well lead to reactivity that is distinct from that of the corresponding organohalides in nickel-catalysed cross-coupling reactions, and so here we systematically examine the reactions of a series of aryl and vinyl triflates with **1**.

Results and discussion

Product studies

The reactions of [Ni(COD)(dppf)] (**1**) with phenyl triflate (**2c**), cyclopent-1-en-1-yl triflate (**5a**), cyclohex-1-en-1-yl triflate (**5b**), cyclohept-1-en-1-yl triflate (**5c**), and cyclooct-1-en-1-yl triflate (**5d**) lead ultimately to [Ni(OTf)(dppf)] (**6**) as confirmed by EPR spectroscopic analysis (Scheme 1 and Fig. 1). The organic fragment of the organotriflate ultimately forms the

[a] *Department of Pure and Applied Chemistry, University of Strathclyde, 295 Cathedral Street, Glasgow, G1 1XL, UK. E-mail: david.nelson@strath.ac.uk*
[b] *Chemical Development, Pharmaceutical Technology and Development, Operations, AstraZeneca, Macclesfield, SK10 2NA, UK*
[c] *School of Chemistry, University of Glasgow, University Avenue, Glasgow, G12 9QQ, UK*
† These authors contributed equally.
‡ Current address for MEG: Sygnature Discovery, Bio City, Pennyfoot Street, Nottingham NG1 1GR, UK.

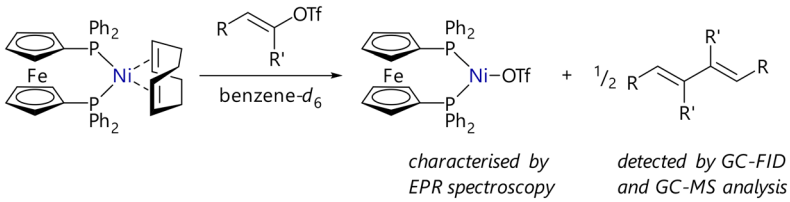

Scheme 1 Reactions of [Ni(COD)(dppf)] (**1**) with phenyl (**2c**), cyclopent-1-en-1-yl (**5a**), cyclohex-1-en-1-yl (**5b**), cyclohept-1-en-1-yl (**5c**), and cyclooct-1-en-1-yl triflate (**5d**).

corresponding homocoupling by-product as confirmed by analysis of the reaction mixture by GC-MS. In the case of **5a** this was confirmed using an authentic sample of this by-product which was prepared by an alternative route.§ The corresponding reactions between **1** and naphthalen-1-yl triflate (**2d**) and 2-pyridyl triflate (**2b**) are known to lead to [Ni(OTf)(1-naphthyl)(dppf)][13] (**7d**) and [Ni(κ²-*C*,*N*-2-pyridyl)(dppf)][OTf][16] (**4**), respectively.

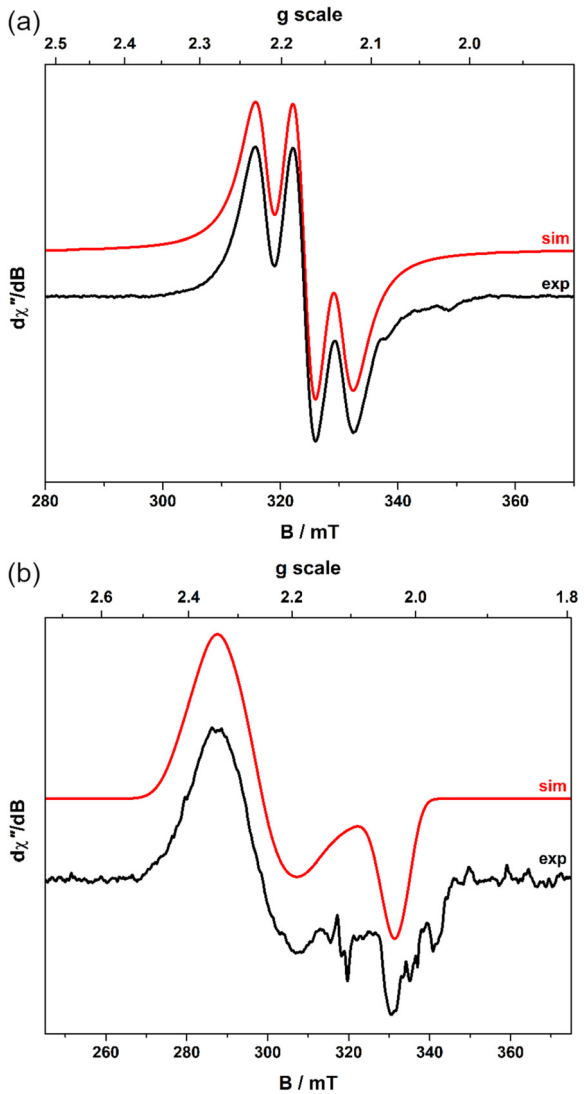

Fig. 1 X-band EPR spectra of [Ni(OTf)(dppf)] (**6**) in THF. (a) Spectrum at 293 K (frequency, 9.8593 GHz; power, 6.3 mW; modulation, 0.6 mT) showing g_{iso} = 2.173 and A_{iso} = 65 × 10^{-4} cm^{-1}. (b) Spectrum at 77 K (frequency, 9.4215 GHz; power, 2.0 mW; modulation, 0.7 mT) showing g = (2.340, 2.265, 2.035) and A = (80, 80, 30) × 10^{-4} cm^{-1}. Experimental spectra are in black (bottom) and simulations are shown in red (at the top).

Kinetic studies

Kinetic studies of the oxidative addition step were conducted using $^{31}P\{^{1}H\}$ NMR spectroscopy in a manner analogous to our previous studies.[13,15–18] A solution of [Ni(COD)(dppf)] (**1**) in benzene-d_6 was prepared in a septum-fitted NMR tube under an argon atmosphere. The organotriflate substrate was added, in excess, *via* syringe and the reaction was monitored at time points within the temperature-controlled cavity of the NMR spectrometer. We elected to conduct these reactions at a lower concentration of **1** after noting that, at 0.022 mol L^{-1}, **1** was not fully solubilised in the presence of the organotriflate and that the reactions were rather fast; a concentration of 0.007 mol L^{-1} was used instead. This was achieved by preparing stock solutions in the glovebox which were then dispensed into NMR tubes under an argon atmosphere before removal from the glovebox and analysis on the spectrometer. Spectra were obtained until *ca.* 85% conversion, corresponding to approximately three half-lives. At the end of the reaction, the characteristic signal for **1** (δ_P = 34 ppm) had almost completely disappeared.

Data were initially processed by plotting the integral of the signal corresponding to **1** *versus* time. Our previous studies had shown that, under conditions where the substrate was present in ten-fold excess with respect to **1**, reactions follow pseudo-first order behaviour and a plot of ln(peak area) *versus* time gave a straight line. However, this was not always observed here (*vide infra*). We consider each class of substrate in turn, but oxidative addition rates are summarised in Table 1.

Phenyl triflate (2c). Consistent with previous observations using *p*-$(F_3C)C_6H_4OTf$ (**2a**), the reactions of phenyl triflate (**2c**) showed good first order behaviour; k_{obs} was determined to be 2.91(5) × 10^{-4} s^{-1} at 323 K based on two replicates (Fig. 2). This was compared to chlorobenzene (**8**) and phenyl tosylate (**9**) under the same conditions, revealing reactivity that decreases in the order PhOTf (k_{rel} = 1.9) > PhCl (k_{rel} = 1.0) > PhOTs (k_{rel} = 0.9). This is slightly different from the order of reactivity established with the

§ Please see the SI for further information.

Table 1 Summary of outcomes from kinetic studies of the reactions of [Ni(COD)(dppf)] (**1**) with organotriflate, organotosylate, and organohalide substrates[a]

Substrate		T (K)	Replicate 1		Replicate 2		Mean	
			k_{obs} (s^{-1})	$t_{1/2}$ (s)	k_{obs} (s^{-1})	$t_{1/2}$ (s)	k_{obs} (s^{-1})	$t_{1/2}$ (s)
Phenyl triflate	**2c**	323	2.95×10^{-4}	2350	2.86×10^{-4}	2424	$2.91(5) \times 10^{-4}$	2382
Chlorobenzene	**8**	323	1.51×10^{-4}	4587	1.49×10^{-4}	4652	$1.50(1) \times 10^{-4}$	4621
Phenyl tosylate	**9**	323	1.30×10^{-4}	5325	1.33×10^{-4}	5222	$1.31(2) \times 10^{-4}$	5274
2-Pyridinyl triflate[b]	**2b**	293	n.d.	2100	n.d.	2100	n.d.	2100
3-Pyridinyl triflate	**2d**	293	3.73×10^{-3}	185	3.82×10^{-3}	182	$3.78(5) \times 10^{-3}$	183
Cyclopent-1-en-1-yl triflate	**5a**	323	6.06×10^{-4}	1144	6.10×10^{-4}	1136	$6.08(2) \times 10^{-4}$	1140
Cyclohex-1-en-1-yl triflate	**5b**	333	6.94×10^{-4}	999	6.86×10^{-4}	1010	$6.90(4) \times 10^{-4}$	1005
Cyclohept-1-en-1-yl triflate	**5c**	323	7.59×10^{-4}	913	8.04×10^{-4}	862	$7.8(2) \times 10^{-4}$	889
Cyclooct-1-en-1-yl triflate	**5d**	323	5.46×10^{-4}	1270	5.65×10^{-4}	1227	$5.6(1) \times 10^{-4}$	1249

[a] Unless otherwise stated, half-lives are obtained from the corresponding pseudo-first order rate constant ($t_{1/2} = \ln(2)/k_{obs}$). [b] Half-life estimated from a plot of integral *versus* time; the reaction does not exhibit well-behaved (pseudo-)first order kinetic behaviour.

para-trifluoromethylphenyl analogues. In our earlier study, compared to the aryl chloride, the relative rates of reaction were 0.15 and 0.35 for the triflate and the tosylate, respectively.[13] In this 2017 study we noted a rather odd two-phase Hammett plot which suggested that both electron-rich and electron-poor substrates react more slowly than the parent phenyl substrate; the region of the plot between $\sigma_p = 0$ and $\sigma_p = 0.45$ was not explored fully due to a discovery that aldehydes and ketones were privileged in this reaction.[15,21] A fuller exploration of this behaviour will form the subject of a subsequent study.

Pyridinyl triflates (2b, 2d). We successfully prepared§ 2-pyridinyl triflate (**2b**) and 3-pyridinyl triflate (**2d**) but were unable to obtain a sufficiently pure sample of 4-pyridinyl triflate (**2e**). These reactions behave somewhat differently to those of aryl triflates, but there is substantial precedent for different behaviours and mechanisms for the oxidative addition of heteroaryl *vs.* aryl (pseudo)halides to low valent transition metals. For example, Jutand has established that pyridinyl halides and aryl halides behave rather differently in oxidative addition reactions with palladium(0), with the former undergoing an S_NAr-type mechanism and the latter a concerted mechanism.[9] Leitch has developed a quantitative structure–activity model that predicts barriers and preferred mechanisms for a large number of (hetero)aryl halides and (hetero)aryl triflates.[11,12] In Leitch's recent study, 2-pyridyl triflate was found to have an anomalous oxidative addition transition state in which there was a very long Pd···N distance; this lacked an interaction between palladium and the triflate fragment, consistent with a displacement mechanism.[12] Neufeldt has noted the proclivity of triflate substrates for displacement-type transition states on the basis of the stability of the triflate anion and ineffective coordination of the oxygen atoms in triflate to palladium.[10] We have previously shown that 2-pyridinyl substrates can lead to the sequestration of nickel catalysts.[16]

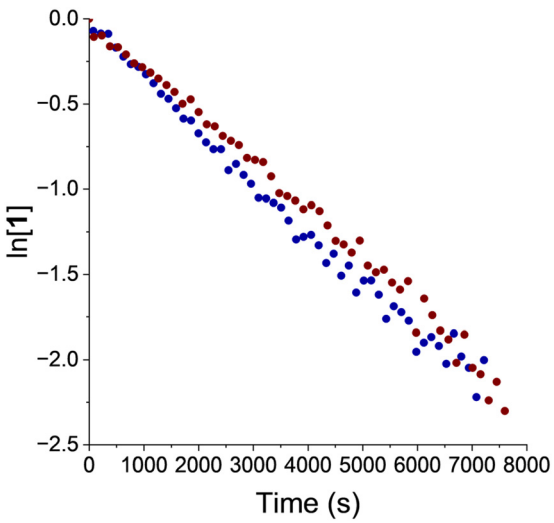

Fig. 2 ln[**1**] *versus* time for the reactions of phenyl triflate (**2c**) (0.14 mol L^{-1}) with [Ni(COD)(dppf)] (**1**) (0.007 mol L^{-1}) at 323 K in benzene-d_6. Each replicate is shown as a separate plot.

The reaction of 2-pyridinyl triflate (**2b**) with **1** has a half-life ($t_{1/2}$) of *ca.* 2100 s at 293 K and occurs approximately one order of magnitude more quickly than the reaction of phenyl triflate (**2c**) ($t_{1/2} \approx 2400$ s at 323 K). However, the reaction of **2b** does not follow expected pseudo-first order behaviour. Instead, the profile of **1** *versus* time appears to show a short induction period followed by approximately zero order behaviour (Fig. 3(a)). The reactions of 3-pyridinyl triflate (**2d**) are substantially faster and show somewhat less of a deviation from the expected pseudo-first order behaviour; the half-life of this reaction is somewhat surprisingly only *ca.* 180 s at a temperature of 293 K.

Further work was carried out using visual time normalisation analysis (VTNA).[22] Additional kinetic experiments were carried out with $[\mathbf{1}]_0 = 0.0035$ mol L^{-1} and $[\mathbf{2b}]_0 = 0.14$ mol L^{-1}, and with $[\mathbf{1}]_0 = 0.007$ mol L^{-1} and $[\mathbf{2b}]_0 = 0.07$ mol L^{-1} and 0.035 mol L^{-1}. All of these reactions gave profiles of [**1**] *versus* time that were of a similar shape (see the SI). The application of a VTNA treatment gave the rate eqn (1).

$$\text{Rate} = k[\mathbf{1}]^{0.9}[\mathbf{2b}]^{0.3} \quad (1)$$

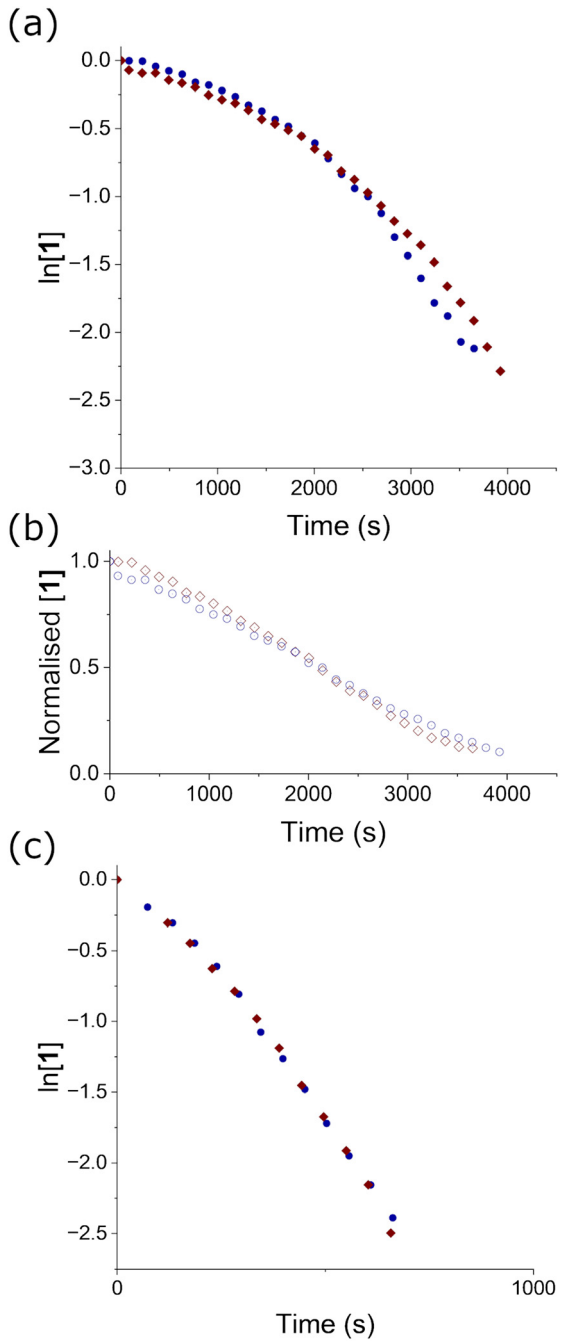

Fig. 3 (a) ln[**1**] *versus* time and (b) normalised integral for **1** *versus* time for the reactions of 2-pyridinyl triflate (**2b**). (c) ln[**1**] *versus* time for the reactions of 3-pyridinyl triflate (**2d**). In each case, 0.14 mol L^{-1} of the substrate was exposed to [Ni(COD)(dppf)] (**1**) (0.007 mol L^{-1}) at 293 K in benzene-d_6. Data for two independent reactions are shown (red diamonds/blue circles).

The ability of this treatment to account for all species that influence the rate of the reaction was tested by plotting the estimated concentration of [Ni(OTf)(dppf)] (**6**) at each time point *versus* the adjusted time for that point. The concentration of **6** was estimated as the difference between the initial concentration of **1** and the concentration of **1** at that time point (*i.e.* eqn (2)).

$$[\mathbf{6}] \approx [\mathbf{1}]_0 - [\mathbf{1}]_{tT} \quad (2)$$

However, the resulting plot once these orders are accounted for does not give a straight line, and therefore there must be another species or process that is influencing the rate of the reaction, for which the effect is time dependent (Fig. 4). At this stage we do not know what this species might be.

Vinyl triflates (5a–d). Intrigued by the possible role of alkene coordination in the rate and selectivity of nickel-catalysed reactions,[14,15] four vinyl triflate substrates were prepared§ from the corresponding cycloalkenones.[5] The oxidative addition reactions were studied using the same kinetic methodology. The reactions showed acceptable and reproducible pseudo-first order behaviour, albeit with slight curvature in plots of ln[**1**] *versus* time, with the most pronounced curvature for the reactions with cyclohex-1-en-1-yl triflate (**5b**) (Fig. 5).

To gain further information on the coordination of alkenes to **1**, we measured equilibrium constants for the displacement of COD by cyclopentene, cyclohexene, cycloheptene, and cyclooctene (Scheme 2). These were obtained by $^{31}P\{^1H\}$ NMR spectroscopic analysis of benzene-d_6 solutions of **1** and each cycloalkene. These equilibrium constants were rather small, as might be expected for the displacement of a bidentate dialkene ligand with a monodentate cycloalkene; K_{eq} decreases in the order cyclopentene > cyclooctene ≈ cycloheptene ≫ cyclohexene. While substrates **5a–d** have additional steric bulk around the alkene, the reticence of cyclohexene in coordinating to **1** may explain – at least in part – the low reactivity of **5b** compared to **5a**, **5c**, and **5d**.

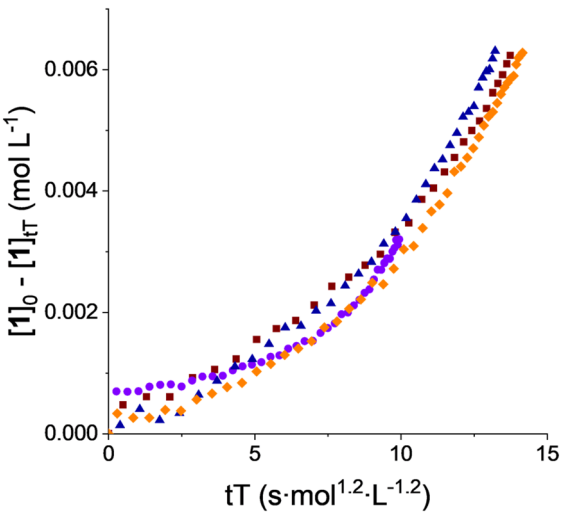

Fig. 4 A VTNA treatment of the reactions of **2b** with **1**, where rate = $k[\mathbf{1}]^{0.9}[\mathbf{2b}]^{0.3}$, using $[\mathbf{1}]_0 - [\mathbf{1}]_{tT}$ as an estimate of the concentration of [Ni(OTf)(dppf)] (**6**). Conditions: 0.007 mol L^{-1} **1**, 0.14 mol L^{-1} **2b** (red squares); 0.0035 mol L^{-1} **1**, 0.14 mol L^{-1} **2b** (purple circles); 0.007 mol L^{-1} **1**, 0.07 mol L^{-1} **2b** (blue triangles); 0.007 mol L^{-1} **1**, 0.035 mol L^{-1} **2b** (orange diamonds). All reactions were conducted at 293 K.

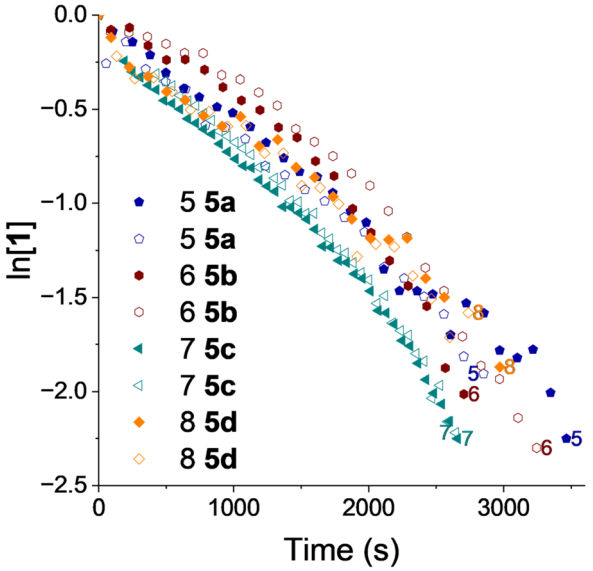

Fig. 5 ln[**1**] *versus* time for the reactions of: cyclopent-1-en-1-yl triflate (**5a**) at 323 K (blue pentagons); cyclohex-1-en-1-yl triflate (**5b**) at 333 K (red hexagons); cyclohept-1-en-1-yl triflate (**5c**) at 323 K (cyan triangles); and cyclooct-1-en-1-yl triflate (**5d**) at 323 K (orange diamonds). Conditions: substrate (0.14 mol L^{-1}) and [Ni(COD)(dppf)] (**1**) (0.007 mol L^{-1}) in benzene-d_6 at the indicated temperature. Open and shaded plots refer to replicates of reactions under the same conditions.

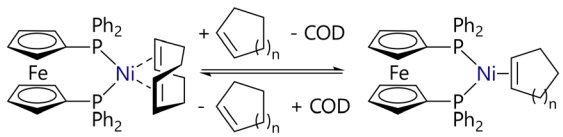

$n = 1$ $K_{eq} = 2.5 \times 10^{-2}$ $n = 3$ $K_{eq} = 5.8 \times 10^{-3}$
$n = 2$ $K_{eq} < 5.1 \times 10^{-4}$ $n = 4$ $K_{eq} = 1.1 \times 10^{-2}$

Scheme 2 Measurement of K_{eq} for the displacement of COD from [Ni(COD)(dppf)] (**1**) by cyclopentene, cyclohexene, cycloheptene, and cyclooctene.

Computational studies

To support our experimental work, a series of computational studies were carried out at the ωB97M-V/ma-Def2-QZVP/SMD(benzene)//r^{2}SCAN-3c level of theory[23–26] using ORCA 6.[27–29] full details regarding methodology can be found in the SI.§ Dispersion is handled for r^{2}SCAN-3c *via* an integrated empirical D4 treatment,[26] while ωB97M-V treats dispersion using the VV10 non-local correlation.[23]

Geometry optimisations were carried out without a solvent model, but solvent effects were included in single point calculations using the SMD model[25] (for benzene solvent). Attempts to optimise structures with a solvent model led to difficulty converging structures with the correct number of imaginary frequencies, and some S_N-type transition states could not be located at all, even with careful scanning of changes to (*e.g.*) key bond distances.

Selected structures were examined at the ωB97M-V/ma Def2-QZVP/SMD(benzene)//ωB97M-V/ma-Def2-SVP level of theory for comparison, but structures and energies were very similar (within 1 kcal mol^{-1}).

A brief benchmarking study was carried out, as described in the SI, to evaluate a number of levels of theory for the single point calculations. ωr^{2}SCAN-D4 and ωB97M-V showed the best performance, with the latter selected due to its use of a non-local correlation method for the treatment of dispersion and the fact that is accepted to be a well-tested and robust functional.

All quoted energies are free energies, in kcal mol^{-1}, with respect to [Ni(COD)(dppf)] (**1**). While it is common practice to apply a correction[30] of +1.89 kcal mol^{-1} to each species to reflect a change from a 1 atm standard state to 1 mol L^{-1}, the key steps here – namely ligand exchange and oxidative addition – do not involve changes in molecularity and so this correction was not applied during this work. While substrates were present in excess with respect to **1** (20 equiv.), which can in principle be corrected for, this was consistent across substrates and so a systematic correction will not change the relative barriers for reaction, for example.

Our outline workflow was as follows. DFT calculations were used to obtain an initial structure. CREST (using xTB)[31,32] was used to generate a library of conformers for each structure in turn. This often required the use of constraints: key atoms were fixed in the case of transition states, while in many cases the Cartesian coordinates of the nickel and iron atoms required to be fixed to avoid structures in which the ferrocene became distorted to facilitate an iron–nickel interaction. The electronic energy of each conformer was evaluated using DFT calculations, and those within a 2 kcal mol^{-1} window were selected for a geometry optimisation/frequency calculation to select the lowest energy conformer. The geometry optimisations were carried out at the r^{2}SCAN-3c level of theory – this composite functional includes a finely tuned triple-ζ basis set and ECPs – and single point calculations at ωB97M-V/ma-Def2-QVP/SMD(benzene) further refined the electronic energies.

Cycloalkene binding. Initial calculations sought to reproduce experimental data for cycloalkene binding to nickel; the lowest energy conformations of [Ni(η^2-cyclopentene)(dppf)] (**10a**), [Ni(η^2-cyclohexene)(dppf)] (**10b**), [Ni(η^2-cycloheptene)(dppf)] (**10c**), and [Ni(η^2-cyclooctene)(dppf)] (**10d**) were identified and $\Delta G°$ was calculated for exchange of COD for the respective cycloalkene; Table 2 lists these data, as well as $\Delta H°$ for comparison. These calculated free energy changes show close agreement with the experimentally measured values, being within 1 kcal mol^{-1} for cyclopentene, cycloheptene, and cyclooctene. Cyclohexene binding is considerably less favourable, consistent with our inability to measure this equilibrium constant experimentally. The free energy differences can be attributed largely to the enthalpy change of this exchange.

Table 2 Calculated ΔH° and ΔG° for displacement of COD from [Ni(COD)(dppf)] (**1**) by cycloalkenes, and experimental ΔG° obtained from $^{31}P\{^1H\}$ NMR spectroscopic analysis of mixtures of **1** and the corresponding cycloalkene

	Experiment		Calculation		
Cycloalkene	K_{eq}	ΔG° (kcal mol^{-1})	ΔH° (kcal mol^{-1})	ΔG° (kcal mol^{-1})	K_{eq}
Cyclopentene	2.5×10^{-2}	2.2	4.9	2.6	1.4×10^{-2}
Cyclohexene	$<5.1 \times 10^{-4}$	>4.5	8.5	6.0	4.0×10^{-5}
Cycloheptene	5.8×10^{-3}	3.0	5.2	3.1	5.3×10^{-3}
Cyclooctene	1.1×10^{-2}	2.7	3.9	1.9	4.2×10^{-2}

Reaction profiles. The free energy profiles for the reactions of phenyl triflate (**2c**), 2- and 3-pyridinyl triflate (**2b**, **2d**), and the set of cycloalk-1-en-1-yl triflates (**5a–d**) were evaluated at ωB97M-V/ma-Def2-QZVP/SMD(benzene)//r^{2}SCAN-3c. These profiles are presented in Fig. 6 and 7. CYLVIEW was used to prepare images of transition states.

Phenyl triflate (**2c**) is considered first, to provide something of a baseline (Fig. 6(a)). The formation of a productive η^2-complex – *i.e.* coordination of nickel to the *ipso*- and *ortho*-positions – is somewhat endergonic (**e2-PhOTf**, G_{rel} = 11.3 kcal mol^{-1}); coordination of nickel to the arene in other positions is less favourable (G_{rel} = 12.1–15.1 kcal mol^{-1}).§ Oxidative addition then takes place *via* either an S_N-type transition state (**TS$_{SN}$-PhOTf**, $\Delta G^\ddagger$ = 14.4 kcal mol^{-1}) or five-centred transition state (**TS$_{5c}$-PhOTf**, $\Delta G^\ddagger$ = 15.6 kcal mol^{-1}). While the former appears to be slightly more favourable, we note that $\Delta\Delta G^\ddagger$ is of the same order of magnitude as the expected error in DFT calculations; we are wary of drawing conclusions based on free energy differences of <2 kcal mol^{-1} and would certainly avoid doing so for free energy differences of <1 kcal mol^{-1}. The ultimate product is then [Ni(Ph)(OTf)(dppf)] (**Ni(II)$_{sp}$-PhOTf**), which is formed irreversibly (G_{rel} = −21.3 kcal mol^{-1}).

The profile for the oxidative addition of 2-pyridinyl triflate (**2b**) are somewhat similar, albeit with more favourable coordination and lower oxidative addition barriers (Fig. 6(b)). Twelve regioisomers of the corresponding η^2-complexes were considered, of which four (per substrate) involve coordination to the carbon atom to which the triflate is attached. The lowest energy isomer is where η^2-coordination takes place at the 3- and 4-positions (**e2b-2PyOTf**, G_{rel} = 7.6 kcal mol^{-1}), and rearrangement to coordination at the 1- and 2-positions (**e2a-2PyOTf**, G_{rel} = 8.5 kcal mol^{-1}) sets the scene for oxidative addition. There is a clear preference for S_N-type oxidative addition (**TS$_{SN}$-2PyOTf**, $\Delta G^\ddagger$ = 6.7 kcal mol^{-1} *cf.* 8.9 kcal mol^{-1} for **TS$_{5c}$-2PyOTf**).¶ This forms a square-based pyramidal [Ni(2-py)(OTf)(dppf)] complex (**Ni(II)$_{sbp}$-2PyOTf**, G_{rel} = −23.0 kcal mol^{-1}), which is slightly lower in energy than the expected square-planar species (**Ni(II)$_{sp}$-2PyOTf**, G_{rel} = −21.0 kcal mol^{-1}). The Ni–O bond is substantially longer in the former than the latter (2.31 Å *versus* 1.95 Å, respectively), consistent with the earlier reported observation that oxidative addition of **2b** to **1** affords [Ni(2-py)(dppf)][OTf] in which the triflate moiety is an outer-sphere anion in the solid state.[16] The Ni–O distance is less than the sum of the van der Waals radii for nickel (2.40 Å) and oxygen (1.50 Å) reported by Alvarez.[33] The coordination of one or two molecules of **2b** to the [Ni(dppf)] fragment, *via* the electron lone pair(s) on the nitrogen atom(s), gave complexes that were higher in energy than the η^2-complexes (>20 kcal mol^{-1}) which are therefore unlikely to be relevant to the oxidative addition mechanism.

For 3-pyridinyl triflate, the situation is slightly different. The lowest energy η^2-complex features nickel coordinated to the 2- and 3-positions (**e2c-3PyOTf**, G_{rel} = 8.9 kcal mol^{-1}); the lowest energy pathway for five-centred oxidative addition proceeds *via* this structure and a subsequent transition state (**TS$_{5c}$-3PyOTf**, $\Delta G^\ddagger$ = 15.8 kcal mol^{-1}) to an undistorted square-planar [Ni(3-py)(OTf)(dppf)] complex (**Ni(II)$_{sp}$-3PyOTf**, G_{rel} = −24.1 kcal mol^{-1}). However, S_N-type oxidative addition offers a lower energy pathway, proceeding through an η^2-complex with coordination at positions 3- and 4- (**e2a-3PyOTf**, G_{rel} = 9.4 kcal mol^{-1}) and a transition state at 14.3 kcal mol^{-1} (**TS$_{SN}$-3PyOTf**), again giving an undistorted square-planar nickel(II) product. It therefore appears that 3-pyridinyl triflate behaves somewhat similarly to phenyl triflate, while the reaction of 2-pyridinyl triflate benefits from a substantial rate increase and leads to a rather different nickel(II) product.

The reactions of the cycloalk-1-en-1-yl triflates differ from those of the hetero(aryl) triflates in that the initial η^2-complex is favourable or close to energetically neutral. The coordination of the alkenyl triflate to nickel is, in each case, more favourable than the coordination of the corresponding cycloalkene (by 4.2–5.6 kcal mol^{-1}), despite the larger steric impact of the triflate substrates that feature trisubstituted rather than *cis*-disubstituted alkenes. This may result from the electron-withdrawing effect of the triflate functional group; $\Delta\Delta G^\circ$ for cycloalkene *versus* substrate binding is somewhat uniform across the four substrates which would support this. Barriers to oxidative addition are substantially lower as a result.

For cyclopent-1-en-1-yl triflate (**5a**) the reaction proceeds *via* favourable exchange of COD (to give **e2-5OTf**, G_{rel} = −3.0

¶ The slightly lower energy of the oxidative addition transition state compared to that of the preceding η^2-complex may be an artefact of the inclusion of solvent effects using a single point calculation; geometry optimisation was carried out without a solvent model. The structure of this η^2-complex was obtained by following the IRC from the transition state.

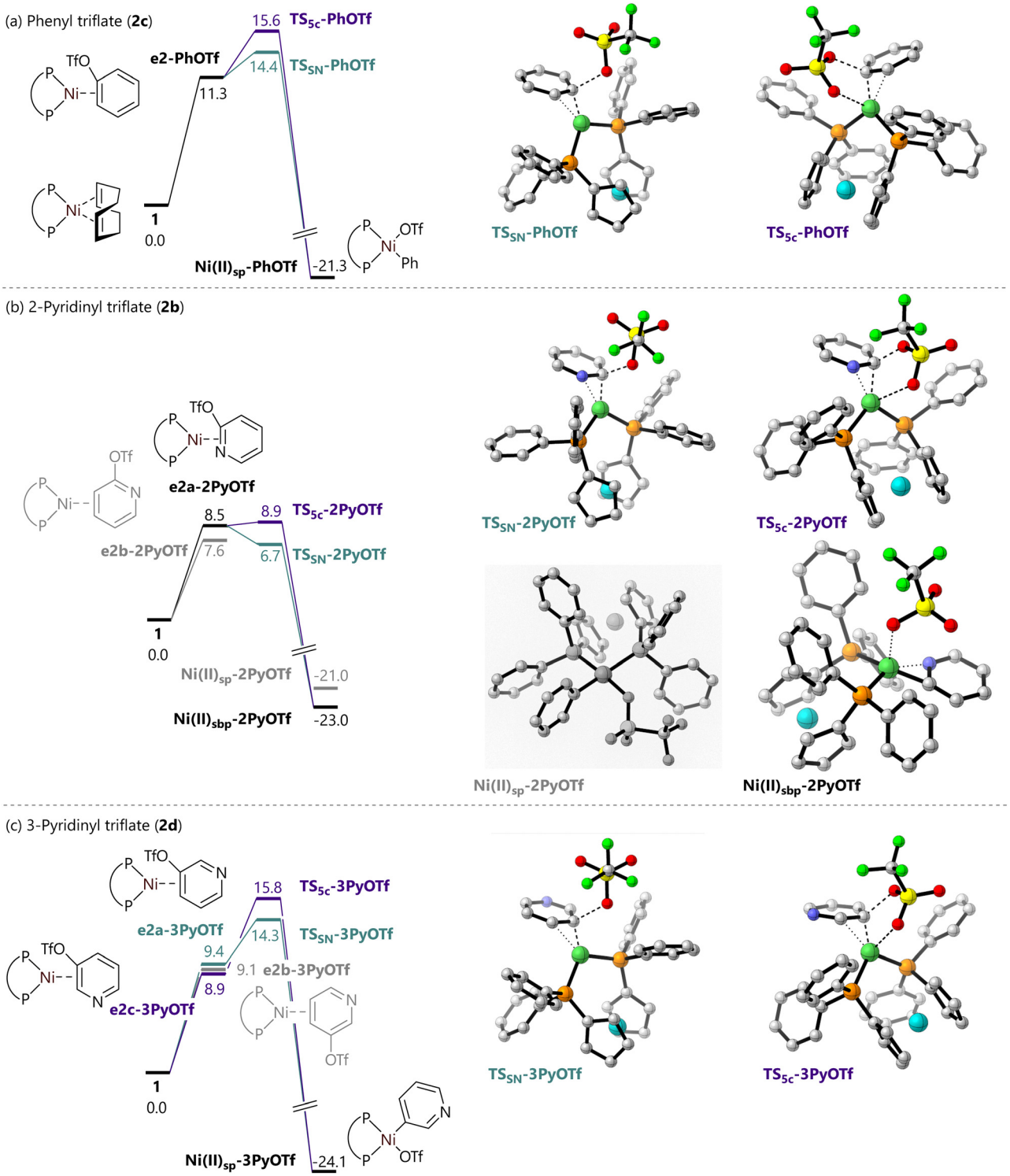

Fig. 6 Free energy profiles for the reactions of (a) phenyl triflate (**2c**), (b) 2-pyridinyl triflate (**2b**), and (c) 3-pyridinyl triflate (**2d**) with [Ni(COD)(dppf)] (**1**). All energies are free energies in kcal mol^{-1} at the ωB97M-V/ma-Def2-QZVP/SMD(benzene)//r^{2}SCAN-3c level of theory, with respect to **1** plus the appropriate substrate **2**.

kcal mol^{-1}) and an S_N-type transition state (**TS$_{SN}$-5OTf**, $\Delta G^{\ddagger}$ = 9.3 kcal mol^{-1}), yielding [Ni(C$_5$H$_9$)(dppf)][OTf] in which the triflate ion is, at best, very loosely bound to the nickel complex (**Ni(II)$_{os}$-5OTf**, G_{rel} = −2.3 kcal mol^{-1}); the Ni–O distance of 3.60 Å is very close to the sum of van der Waals radii for these two elements.[33] **Ni(II)$_{os}$-5OTf** can rearrange to give the expected [Ni(C$_5$H$_9$)(OTf)(dppf)] product (**Ni(II)$_{sp}$-5OTf**, G_{rel} = −20.1 kcal mol^{-1}). The alternative five-centre transition state is a little higher in energy (**TS$_{5c}$-5OTf**, $\Delta G^{\ddagger}$ = 10.8 kcal mol^{-1}). The possible binding of two

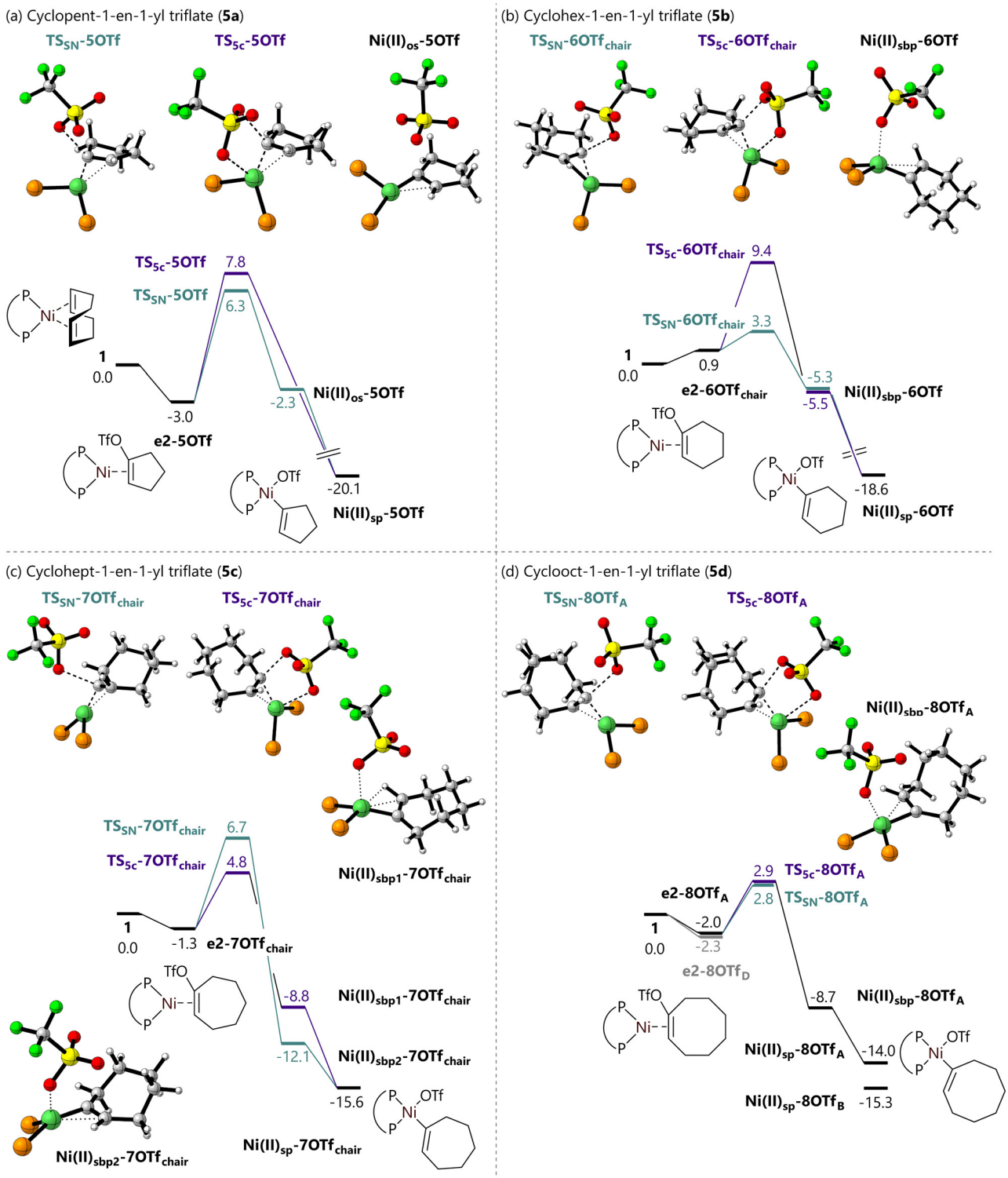

Fig. 7 Free energy profiles for the reactions of (a) cyclopent-1-en-1-yl triflate (**5a**), (b) cyclohex-1-en-1-yl triflate (**5b**), (c) cyclohept-1-en-1-yl triflate (**5c**), and (d) cyclooct-1-en-1-yl triflate (**5d**) with [Ni(COD)(dppf)] (**1**). All energies are free energies in kcal mol^{-1} at the ωB97M-V/ma-Def2-QZVP/SMD(benzene)//r^{2}SCAN-3c level of theory, with respect to **1** plus the appropriate substrate **5**.

molecules of **5a** to the dppf-nickel(0) fragment was investigated, but this was found to be energetically unfeasible (>30 kcal mol^{-1} with respect to **1** plus two molecules of **5a**).

The reaction of cyclohex-1-en-1-yl triflate (**5b**) can proceed *via* intermediates in which the cyclohexene ring adopts a boat or a chair conformation; reactions *via* chair conformations present the lowest energy pathways.§ The coordination of **5b**

is slightly endergonic (**e2-6OTf$_{chair}$**, G_{rel} = 0.9 kcal mol^{-1}), and is followed by an S_N-type transition state (**TS$_{SN}$-6OTf$_{chair}$**, $\Delta G^{\ddagger}$ = 3.3 kcal mol^{-1}) that leads to a distorted square-based pyramidal [Ni(C_6H_9)(OTf)(dppf)] complex (**Ni(II)$_{sp}$-6OTf$_{chair}$**, G_{rel} = −5.3 kcal mol^{-1}) with a clear Ni–O bond (2.19 Å) in the apical position. This can rearrange to the expected square planar species (**Ni(II)$_{sp}$-6OTf$_{chair}$**, −18.6 kcal mol^{-1}). The alternative five-centred transition state is substantially higher in energy and therefore uncompetitive (**TS$_{5c}$-6OTf$_{chair}$**, $\Delta G^{\ddagger}$ = 9.4 kcal mol^{-1}). The very low barrier to SN-type oxidative addition here was somewhat surprising, given the experimental data showing that this substrate is rather reticent in oxidative addition to nickel(0).

In the case of cyclohept-1-en-1-yl triflate (**5c**) the most favourable pathways again involve chair rather than boat conformations of the cycloheptene ring.§ A moderately favourable exchange of COD for **5c** (**e2-7OTf$_{chair}$**, G_{rel} = −1.3 kcal mol^{-1}) is followed by a five-centered oxidative addition transition state (**TS$_{5c}$-7OTf$_{chair}$**, $\Delta G^{\ddagger}$ = 6.1 kcal mol^{-1}), leading to a distorted square planar [Ni(C_7H_{11})(OTf)(dppf)] complex (**Ni(II)$_{sbp1}$-7OTf$_{chair}$**, G_{rel} = −8.8 kcal mol^{-1}) that can then rearrange to give the expected square planar [Ni(C_7H_{11})(OTf)(dppf)] product (**Ni(II)$_{sp}$-7OTf$_{chair}$**, −15.6 kcal mol^{-1}). The S_N-type transition state is less favourable (**TS$_{SN}$-7OTf$_{chair}$**, $\Delta G^{\ddagger}$ = 8.0 kcal mol^{-1}).

Finally, four possible conformations for cyclooct-1-en-1-yl triflate were considered, and the corresponding S_N-type and five-centred oxidative addition pathways were modelled. Conformational screening was facilitated by the use of xTB and CREST[31,32,34] and literature regarding the conformational analysis of cyclooctene;[35] Neuenschwander and Hermans have identified four conformations of cyclooctene which they have labelled A–D, and the same nomenclature is adopted here.[35] Only the *cis*-cyclooctene was considered, as *trans*-cyclooctenes are substantially more strained.[36] The η^2-complex with conformation D is the lowest in energy (**e2-8OTf$_{D}$**, G_{rel} = −2.3 kcal mol^{-1}) but the lowest energy pathway occurs *via* conformation A (**e2-8OTf$_{A}$**, G_{rel} = −2.0 kcal mol^{-1}). S_N-type and five-centered mechanisms are very close in energy, with barriers that differ by only 0.1 kcal mol^{-1} ($\Delta G^{\ddagger}$ = 2.8 and 2.9 kcal mol^{-1}, respectively, for **TS$_{SN}$-8OTf$_{A}$** and **TS$_{5c}$-8OTf$_{A}$**). In either case, a distorted square-based pyramidal nickel(II) complex results (**Ni(II)$_{sbp}$-8OTf$_{A}$**, G_{rel} = −8.7 kcal mol^{-1}). The energies of square planar nickel(II) complexes with cyclooctene fragments in conformations A, B, C, and D are rather close, at −14.0, −15.3, −12.7, and −13.6 kcal mol^{-1}, respectively (**Ni(II)$_{sp}$-8OTf$_{X}$**).

Overall, these substrates can be considered in three groups. [1] Phenyl triflate (**2c**) and 3-pyridinyl triflate (**2d**) appear to have the highest barriers to oxidative addition, which largely appears to be a result of the need to displace COD from [Ni(COD)(dppf)] (**1**) with substrates that are poorer ligands. This will be more of a challenge for catalyst systems that involve COD or other strongly-binding ligands, but less of an issue for catalyst systems where no such competing ligands are present. These substrates have a modest preference for S_N-type oxidative addition rather than a five-centred transition state. [2] 2-Pyridinyl triflate (**2b**) has a much lower barrier to oxidative addition, which can be partly – but not fully – attributed to the much more favourable coordination of the substrate to nickel(0). This substrate has a strong preference for S_N-type oxidative addition. [3] The cycloalk-1-en-1-yl triflate substrates coordinate readily to nickel(0) – to different extents, depending on ring size and conformation – and undergo oxidative addition with much lower barriers. It is possible then that the oxidative addition rate might rely, at least to some extent, on the rate at which ligand exchange occurs at nickel(0). The preferred mechanism for oxidative addition varies depending on the substrate.

Catalytic cross-coupling reactions

A representative set of aryl and vinyl triflates was deployed in Kumada–Tamao–Corriu cross-coupling reactions to confirm that **1** is competent for the cross-coupling reactions of these substrates (Scheme 3). These conditions are unoptimised, but were previously deployed for the cross-coupling of alkyl halides with aryl Grignard reagents, and use only 1.1 equivalents of the latter.[17,18] Reaction yields were quantified *versus* an internal standard by GC-FID analysis which was calibrated using authentic samples of each product; a substituted aryl triflate (**2a**) was used rather than phenyl triflate (**2c**) in order to distinguish between cross- and homo-coupling processes. The reactions proceeded in moderate to excellent yields, confirming the competence of this catalyst system. There is not a correlation between oxidative addition rate and reaction yield, but these are single point yield measurements from catalytic reactions carried out at a higher temperature and for a longer time

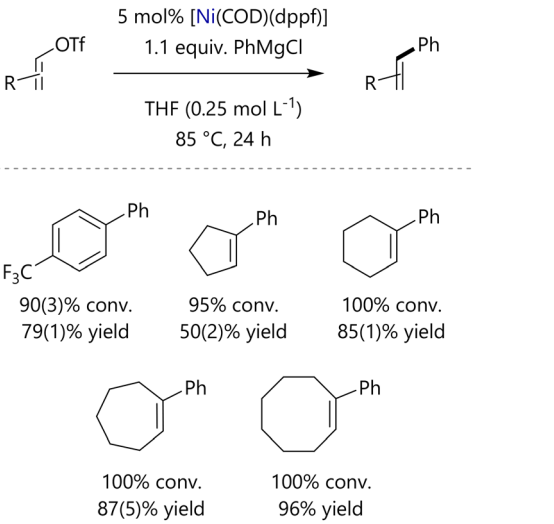

Scheme 3 Nickel-catalysed cross-coupling reactions of aryl and alk-1-en-1-yl triflates. Reactions were assayed by calibrated GC-FID analysis.

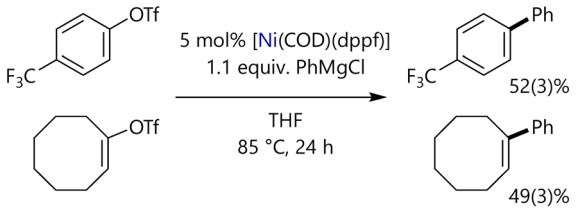

Scheme 4 Competitive cross-coupling experiment to probe any correlation between oxidative addition rate and selectivity. Reactions were assayed by calibrated GC-FID analysis.

period than the oxidative addition studies. The rather low yield of 1-phenyl-cyclopentene is an outlier, and the fate of the missing 45% of the substrate is unclear at this stage; this may be due to formation of cyclopentene, which is sufficiently volatile to be lost in the solvent front during GC-FID analysis.

Finally, we wished to identify whether the more favourable coordination of alkenyl triflates to nickel(0) (compared to aryl triflates) might allow a selective cross-coupling reaction to be achieved. Reactions were carried out in which one equivalent of each of 4-(trifluoromethyl)phenyl triflate (**2a**) and cyclooct-1-en-1-yl triflate (**5d**) were exposed to 1.1 equivalents of phenylmagnesium chloride and 5 mol% of [Ni(COD)(dppf)]; these reactions were surprisingly unselective, and produced the corresponding products in approximately equal yield (Scheme 4). This may have several explanations, for example: (i) oxidative addition is reversible, which has been suggested in other studies[37] but seems inconsistent with the free energies of reaction calculated here for oxidative addition; or (ii) the rate of oxidative addition might be dependent on the rate of the initial ligand exchange.

Conclusions

This manuscript presents a detailed study of the reactions of (hetero)aryl and cycloalk-1-en-1-yl triflates with the model complex [Ni(COD)(dppf)] (**1**). It is found that the relative rates of oxidative addition follow the approximate trend 3-pyridinyl ≫ cyclohept-1-en-1-yl ≈ cyclopent-1-en-1-yl ≈ cyclooct-1-en-1-yl > cyclohex-1-en-1-yl > 2-pyridinyl > phenyl. However, the kinetic behaviour of some substrates does not follow the expected pseudo-first order behaviour, and a VTNA treatment suggests that additional factors lead to an increase in rate over the course of the oxidative addition experiment.

Computational studies using DFT calculations show a modest preference in most cases for SN-type oxidative addition transition states, with a five-centred transition state being preferred for cyclohept-1-en-1-yl triflate (**5c**). These do not reproduce experimental data well, despite extensive attempts to systematically and fully explore the relevant conformational space; the lower barrier for oxidative addition of 2-pyridinyl triflate (**2b**) *versus* phenyl triflate (**2c**) is consistent with experimental results, but the free energy profile for 3-pyridyl triflate (**2d**) is at odds with the experimental observation that this reaction is very fast. Similarly, the trend for cycloalk-1-en-1-yl triflate reactivity is not reproduced *in silico*. DFT calculations would predict barriers decreasing in the order cyclopent-1-en-1-yl triflate (**5a**) > cyclohept-1-en-1-yl triflate (**5c**) > cyclooct-1-en-1-yl triflate (**5d**) > cyclohex-1-en-1-yl triflate (**5b**). The deviation from pseudo-first order behaviour for the experimental data for **5b** suggests that these reactions also have additional complexity that we do not yet understand.

The results of the competition experiment in Scheme 4 were a little surprising, given the much more favourable coordination of cycloalk-1-en-1-yl triflates *versus* phenyl triflate, and the lower overall barriers to oxidative addition that were calculated. This suggests that displacement of the COD from nickel by the substrate is slow under the reaction conditions, that the oxidative addition step is not selectivity-determining, that the oxidative addition step is reversible, or some combination of these explanations.

There are several possible explanations for this disconnect between experiment and theory; the exploration of these lie outside the scope of the present work.

- The speciation of the active nickel(0) complex may be different; we have shown that alkyl halides, for example, react with [Ni(κ^2-dppf)(κ^1-dppf)] (**10**), even when apparently pure samples of [Ni(COD)(dppf)] (**1**) are used.[17] We do not suspect that **10** is competent for oxidative addition in this system: the steric demand of oxidative addition is considerably larger than that for single electron processes such as halogen abstraction[38,39] or single electron transfer.[40,41]
- Single electron processes may be at play: the reduction potentials of aryl triflates are substantially lower than those of the corresponding aryl halides.[42]
- While we have probed the equilibria involved in ligand exchange at **1**, it is possible that the rates of ligand exchange have an influence. This is very challenging to model accurately using DFT calculations. Luo *et al.* have recently shown that electron-poor vinyl fluoride substrates can be activated in preference to less electron-poor vinyl chlorides (*inter alia*), which is proposed to be due to the rate of ligand exchange at nickel(0).[43]

Further work is underway in our laboratory to understand the reactivity of organotriflates and other organo(pseudo) halides with nickel(0) in further detail.

Author contributions

Conceptualisation: DJN; data curation: NCCM, MEG, SS, DJN; formal analysis: NCCM, MEG, SS, DJN; funding acquisition: RM, TOR, SR, DJN; investigation: NCCM, MEG, SS, DJN; methodology: NCCM, MEG, SS, DJN; project administration: RM, TOR, SR, DJN; resources: SS, DJN; supervision: RM, TOR, SR, DJN; visualisation: DJN; writing – original draft: NCCM, DJN; writing – review & editing: NCCM, MEG, RM, TOR, SR, SS, DJN.

Conflicts of interest

There are no conflicts to declare.

Data availability

Data supporting this article have been included as part of the supplementary information (SI).

Supplementary information: synthesis and characterisation of substrates **2b–d** and **5a–d**; NMR spectroscopy data for kinetic and equilibrium studies; computational methodology, energies, and the geometries of all structures. Additional references are cited in the SI.[44–51] See DOI: https://doi.org/10.1039/d6cy00261g.

Raw experimental data underpinning this article are available from the PURE data repository hosted at the University of Strathclyde, *via* the following DOI: https://doi.org/10.15129/6a36350c-9209-4fd5-a662-38e6911dfc17.

Computational data underpinning this article are available from the ioChem-BD data repository[52] hosted at the Barcelona Supercomputing Centre, *via* the following DOI: https://doi.org/10.19061/iochem-bd-6-653.

Acknowledgements

NCCM, MEG, and DJN thank AstraZeneca and the UK Research and Innovation Engineering and Physical Sciences Research Council (UKRI EPSRC) for studentship funding (EP/W524670/1 and EP/R512114/1). We thank Mr C. Irving, Dr J. Parkinson, Ms P. Keating (retired), and Mr F. McGeoch for assistance with technical and analytical facilities at the University of Strathclyde. Computational calculations reported in this study were conducted using the ARCHIE-WeSt High Performance Computer hosted at the University of Strathclyde (https://www.archie-west.ac.uk), and we thank J. Buzzard, Dr K. Karina-Ossowska, and Dr R. Martin for their assistance with this facility. We thank the referees for their many detailed and constructive suggestions that have improved this manuscript.

Notes and references

1 H. Chen, S. Sun and X. Liao, *Org. Lett.*, 2019, **21**, 3625–3630.
2 F.-F. Pan, P. Guo, C.-L. Li, P. Su and X.-Z. Shu, *Org. Lett.*, 2019, **21**, 3701–3705.
3 L. Su, G. Ma, Y. Song and H. Gong, *Org. Lett.*, 2021, **23**, 2493–2497.
4 X. Wang, F. Liu, Z. Yan, Q. Qiang, W. Huang and Z.-Q. Rong, *ACS Catal.*, 2021, **11**, 7319–7326.
5 J. Duan, Y.-F. Du, X. Pang and X.-Z. Shu, *Chem. Sci.*, 2019, **10**, 8706–8712.
6 Z.-X. Tian, J.-B. Qiao, G.-L. Xu, X. Pang, L. Qi, W.-Y. Ma, Z.-Z. Zhao, J. Duan, Y.-F. Du, P. Su, X.-Y. Liu and X.-Z. Shu, *J. Am. Chem. Soc.*, 2019, **141**, 7637–7643.
7 I. L. Baraznenok, V. G. Nenajdenko and E. S. Balenkova, *Tetrahedron*, 2000, **56**, 3077–3119.
8 M. E. Greaves, E. L. B. Johnson Humphrey and D. J. Nelson, *Catal. Sci. Technol.*, 2021, **11**, 2980–2996.
9 B. U. W. Maes, S. Verbeeck, T. Verhelst, A. Ekomié, N. von Wolff, G. Lefèvre, E. A. Mitchell and A. Jutand, *Chem. – Eur. J.*, 2015, **21**, 7858–7865.
10 M. J. Kania, A. Reyes and S. R. Neufeldt, *J. Am. Chem. Soc.*, 2024, **146**, 19249–19260.
11 J. Lu, S. Donnecke, I. Paci and D. C. Leitch, *Chem. Sci.*, 2022, **13**, 3477–3488.
12 J. Lu, H. Celuszak, I. Paci and D. C. Leitch, *Chem. – Eur. J.*, 2024, **30**, e202402282.
13 S. Bajo, G. Laidlaw, A. R. Kennedy, S. Sproules and D. J. Nelson, *Organometallics*, 2017, **36**, 1662–1672.
14 G. Yin, I. Kalvet, U. Englert and F. Schoenebeck, *J. Am. Chem. Soc.*, 2015, **137**, 4164–4172.
15 A. K. Cooper, D. K. Leonard, S. Bajo, P. M. Burton and D. J. Nelson, *Chem. Sci.*, 2020, **11**, 1905–1911.
16 A. K. Cooper, M. E. Greaves, W. Donohoe, P. M. Burton, T. O. Ronson, A. R. Kennedy and D. J. Nelson, *Chem. Sci.*, 2021, **12**, 14074–14082.
17 M. E. Greaves, T. O. Ronson, G. C. Lloyd-Jones, F. Maseras, S. Sproules and D. J. Nelson, *ACS Catal.*, 2020, **10**, 10717–10725.
18 M. E. Greaves, T. O. Ronson, F. Maseras and D. J. Nelson, *Organometallics*, 2021, **40**, 1997–2007.
19 E. D. Entz, J. E. A. Russell, L. V. Hooker and S. R. Neufeldt, *J. Am. Chem. Soc.*, 2020, **142**, 15454–15463.
20 E. K. Reeves, E. D. Entz and S. R. Neufeldt, *Chem. – Eur. J.*, 2021, **27**, 6161–6177.
21 A. K. Cooper, P. M. Burton and D. J. Nelson, *Synthesis*, 2020, **52**, 565–573.
22 C. D.-T. Nielsen and J. Burés, *Chem. Sci.*, 2019, **10**, 348–353.
23 N. Mardirossian and M. Head-Gordon, *J. Chem. Phys.*, 2016, **144**, 214110.
24 J. Zheng, X. Xu and D. G. Truhlar, *Theor. Chem. Acc.*, 2011, **128**, 295–305.
25 A. V. Marenich, C. J. Cramer and D. G. Truhlar, *J. Phys. Chem. B*, 2009, **113**, 6378–6396.
26 S. Grimme, A. Hansen, S. Ehlert and J.-M. Mewes, *J. Chem. Phys.*, 2021, **154**, 064103.
27 F. Neese, *WIREs Comput. Mol. Sci.*, 2022, **12**, e1606.
28 F. Neese, *WIREs Comput. Mol. Sci.*, 2025, **15**, e70019.
29 F. Neese, *WIREs Comput. Mol. Sci.*, 2012, **2**, 73–78.
30 J. N. Harvey, F. Himo, F. Maseras and L. Perrin, *ACS Catal.*, 2019, **9**, 6803–6813.
31 P. Pracht, S. Grimme, C. Bannwarth, F. Bohle, S. Ehlert, G. Feldmann, J. Gorges, M. Müller, T. Neudecker, C. Plett, S. Spicher, P. Steinbach, P. A. Wesołowski and F. Zeller, *J. Chem. Phys.*, 2024, **160**, 114110.
32 C. Bannwarth, E. Caldeweyher, S. Ehlert, A. Hansen, P. Pracht, J. Seibert, S. Spicher and S. Grimme, *WIREs Comput. Mol. Sci.*, 2021, **11**, e1493.
33 S. Alvarez, *Dalton Trans.*, 2013, **42**, 8617–8636.
34 P. Pracht, F. Bohle and S. Grimme, *Phys. Chem. Chem. Phys.*, 2020, **22**, 7169–7192.
35 U. Neuenschwander and I. Hermans, *J. Org. Chem.*, 2011, **76**, 10236–10240.

36 H. A. Skinner and G. Pilcher, *Q. Rev., Chem. Soc.*, 1963, **17**, 264–288.
37 Y. Ben-Tal and G. C. Lloyd-Jones, *J. Am. Chem. Soc.*, 2022, **144**, 15372–15382.
38 I. Funes-Ardoiz, D. J. Nelson and F. Maseras, *Chem. – Eur. J.*, 2017, **23**, 16728–16733.
39 D. J. Nelson and F. Maseras, *Chem. Commun.*, 2018, **54**, 10646–10649.
40 C. N. Pierson and J. F. Hartwig, *Nat. Chem.*, 2024, **16**, 930–937.
41 T. T. Tsou and J. K. Kochi, *J. Am. Chem. Soc.*, 1979, **101**, 6319–6332.
42 K. Grudzień, A. Zlobin, J. Zadworny, K. Rybicka-Jasińska and B. Sadowski, *Org. Chem. Front.*, 2024, **11**, 5232–5277.
43 Y.-C. Luo, Y.-H. Xu and X. Zhang, *Chin. J. Chem.*, 2026, **44**, 1073–1082.
44 V. J. Olsson and K. J. Szabó, *J. Org. Chem.*, 2009, **74**, 7715–7723.
45 G. R. Fulmer, A. J. M. Miller, N. H. Sherden, H. E. Gottlieb, A. Nudelman, B. M. Stoltz, J. E. Bercaw and K. I. Goldberg, *Organometallics*, 2010, **29**, 2176–2179.
46 X. Su, H. Huang, Y. Yuan and Y. Li, *Angew. Chem., Int. Ed.*, 2017, **56**, 1338–1341.
47 D. E. Frantz, D. G. Weaver, J. P. Carey, M. H. Kress and U. H. Dolling, *Org. Lett.*, 2002, **4**, 4717–4718.
48 T. H. Wöste and M. Oestreich, *Chem. – Eur. J.*, 2011, **17**, 11914–11918.
49 R. M. Oechsner, I. H. Lindenmaier and I. Fleischer, *Org. Lett.*, 2023, **25**, 1655–1660.
50 K. C. Nicolaou, H. Zhang, A. Ortiz and P. Dagneau, *Angew. Chem., Int. Ed.*, 2008, **47**, 8605–8610.
51 J.-H. Li and W.-J. Liu, *Org. Lett.*, 2004, **6**, 2809–2811.
52 M. Álvarez-Moreno, C. de Graaf, N. López, F. Maseras, J. M. Poblet and C. Bo, *J. Chem. Inf. Model.*, 2015, **55**, 95–103.

